

To appear in the Astronomical Journal

QUASARS AS ABSORPTION PROBES OF THE HUBBLE DEEP FIELD¹

Charles T. Liu

Department of Astronomy, Columbia University, New York, NY 10027; and
 Department of Astrophysics, American Museum of Natural History, New York, NY 10024
 email: cliu@astro.columbia.edu; cliu@amnh.org

Cathy E. Petry and Chris D. Impey
 Steward Observatory, The University of Arizona, Tucson, AZ 85721
 email: cpetry@as.arizona.edu, cimpey@as.arizona.edu

and

Craig B. Foltz
 Multiple Mirror Telescope Observatory, The University of Arizona, Tucson, AZ 85721
 email: cfoltz@as.arizona.edu

ABSTRACT

We present a catalog of 30 QSOs and their spectra, in the square degree of sky centered on the northern Hubble Deep Field. These QSOs were selected by multicolor photometry and subsequently confirmed with spectroscopy. They range in magnitude from $17.6 < B < 21.0$ and in redshift from $0.44 < z < 2.98$. We also include in the catalog an AGN with redshift $z=0.135$. Together, these objects comprise a new grid of absorption probes which can be used to study the correlation between luminous galaxies, non-luminous halos and Lyman- α absorbers along the line of sight toward the Hubble Deep Field.

Subject headings: quasars: emission lines — surveys

¹ Observations reported here were obtained at the Multiple Mirror Telescope Observatory, a facility operated jointly by the University of Arizona and the Smithsonian Institution; and at Kitt Peak National Observatory, National Optical Astronomy Observatories, operated by AURA Inc., under contract with the National Science Foundation.

1. INTRODUCTION

The Hubble Deep Field (HDF), with its unprecedented depth and its rich resource of complementary data, has opened new avenues for studying galaxy evolution and cosmology (Williams et al. 1996; Livio, Fall & Madau 1998). The northern HDF no longer stands alone as the subject of the deepest image of the sky ever made; it was recently matched by deep Hubble Space Telescope (HST) observations of a southern field (Williams et al. 1998). In this paper, we use the term HDF to refer only to the northern field. Yet, no matter how deep any imaging survey might be, it can only reveal the luminous parts of galaxies, which comprise only 2-3% of the material in the universe. An examination of the cold, diffuse and dark components of the universe along the line of sight toward the HDF would provide an important complement to the study of the luminous matter content between $0 < z < 4$.

There are a number of benefits to an absorption survey, using distant QSOs as background probes. Material can be detected in absorption that would be impossible to detect in emission. For example, galaxy halos can be detected using the CIV $\lambda\lambda 1548, 1550$ and Mg II $\lambda\lambda 2796, 2800$ doublets over the entire range $0 < z < 4$ (e.g. Meylan 1995). Moreover, quasar absorption can be detected via Lyman- α absorption at an HI column a million times lower than can be seen directly in emission (Rauch 1998). Lyman- α absorbers are as ubiquitous as galaxies and they effectively trace the potential of the underlying dark matter distribution (Hernquist et al. 1996; Miralda-Escudé et al. 1996). Finally, given a sufficiently bright background quasar, absorbers can be detected with an efficiency that does not depend on redshift. By contrast, galaxy surveys are inevitably complicated by effects such as Malmquist bias, cosmological dimming, k-corrections and surface brightness selection effects.

The detection of a network of QSO absorbers in a volume centered on a deep pencil-beam survey allows several interesting experiments in large scale structure. It allows clustering to be detected on scales in excess of $10 h_{100}^{-1}$ Mpc. Individual QSO sightlines show CIV and Mg II correlation power on scales up to $20 h_{100}^{-1}$ Mpc (Quashnock & Vanden Berk 1998), and multiple sightlines have been used to trace out three-dimensional structures on even larger scales (Sargent & Steidel 1987; Dinshaw & Impey 1996; Williger et al. 1996). Deep pencil-beam galaxy redshift surveys have shown that around half of the galaxies lie in structures with line of sight separations of $50-300 h_{100}^{-1}$ Mpc (Cohen et al. 1996, 1999). In addition, the spatial relationship between quasar absorbers and luminous galaxies can be defined; they are expected to have different relationships to the underlying mass distribution (Cen et al. 1998).

We have identified a set of QSOs in the direction of the HDF, suitable for use as background probes of the volume centered on the HDF line of sight. Section 2 contains the multicolor photometry and a simple multicolor QSO selection strategy. Section 3 includes a description of subsequent confirming spectroscopy, a catalog of confirmed QSOs out to $z \approx 3$ in the magnitude range $17 \lesssim B \lesssim 21$, and a discussion of the completeness of the survey and the properties of the confirmed QSOs. Section 4 is a brief summary, along with comments on the applications of these

potential absorption line probes.

2. PHOTOMETRY AND CANDIDATE SELECTION

2.1. Multicolor Photometry

The goal of this study was to obtain a grid of absorption probes out to a radius from the HDF of one cluster-cluster correlation scale length, or about $8 h_{100}^{-1}$ Mpc, at the median redshift of the deep galaxy surveys, $z = 0.8$. For the cosmology we adopt with $H_0 = 100 \text{ km s}^{-1} \text{ Mpc}^{-1}$ and $q_0=0.5$, this corresponds to approximately 30 arcminutes. Our search area was thus the square degree centered on the HDF (B1950.0 12:34:35.5 +62:29:28).

Our first broad-band images of the area centered on the HDF were obtained in March to May 1996, using the Steward Observatory 2.3-meter telescope on Kitt Peak and the Whipple Observatory 1.5-meter telescope on Mt. Hopkins. Poor weather for almost all the observing time on these runs limited the value of these data. Nevertheless, useful U , B , and R band photometry was obtained for 0.12 square degree centered on the HDF. This photometry provided the first QSO candidates for spectroscopic followup, which was conducted April 9-10, 1997 at the Multiple Mirror Telescope on Mt. Hopkins.

Photometry of the complete square degree was ultimately achieved with the KPNO 0.9-meter telescope from April 29 to May 5, 1997. We obtained UBR photometry of the survey area using the T2KA 2048×2048 CCD. With a $23'$ field of view, the entire square degree was covered with a 3×3 mosaic of exposures. Integration times were 60 minutes in the U band, 60 minutes in the B band, and 30 minutes in the R band, each divided into three exposures to facilitate cosmic ray rejection. The seeing for these observations ranged from 1.1 to 2.5 arcseconds FWHM. Images were bias-subtracted, flat-fielded and cleaned of cosmic rays using the standard routines in IRAF. Objects in the reduced images were detected using the Faint Object Classification and Analysis System (FOCAS; Valdes 1982).

Next we used the *apphot* package in IRAF to measure aperture photometry of each object, using a fixed circular aperture 12 pixels ($8''.2$) in diameter and the sky value sampled from an annulus around each object with inner and outer diameters of 16 and 24 pixels respectively. Images in the three filters were registered, and positions were measured using the COORDS task in IRAF, with Hubble Space Telescope guide stars in the frames as a reference grid. The internal rms residuals of the astrometric solutions ranged from $0''.2$ to $0''.5$, which means there was no ambiguity in comparing objects between filters at the magnitude limit of this survey. The computed positions of stars in overlapping regions of the CCD fields matched to within $0''.5$ in all cases.

As with the original imaging observations in the spring of 1996, many of the 0.9-meter observations in 1997 were obtained in non-photometric conditions. Fortunately, enough good

weather was available to obtain flux calibrate each of the U , B and R mosaics under photometric conditions. Absolute photometric calibration was achieved by observing standard stars in the globular clusters NGC 4147 and M 92, which were reduced in the same way as the survey data described above. We used the *photcal* package in IRAF to fit zero points, color terms, and extinction coefficients. The photometric solutions yielded rms errors of 0.02, 0.04 and 0.03 magnitudes respectively for the U , B , and R bands. The 10σ limiting magnitudes for point sources were $U = 21.6$, $B = 22.1$ and $R = 21.8$. In all bands, point sources brighter than ~ 15.5 mag saturated the CCD readout; this was the practical brightness limit for our photometry.

2.2. Candidate Selection

Multicolor selection of QSO candidates is a well understood and widely used technique (e.g., Koo, Kron & Cudworth 1986; Warren et al. 1991; Hall et al. 1996). Essentially, the power law energy distributions of QSOs cause them to be displaced from the stellar locus defined primarily by hot main sequence stars and white dwarfs. For this work, we used a straightforward application of the multicolor selection technique based on $U - B$ and $B - R$ colors. The $U - B$ color provides optimal sensitivity to ultraviolet-excess QSOs at $z < 2$, while the $B - R$ color allows the detection of the rarer objects at high redshift.

Figure 1 shows the $U - B$ vs. $B - R$ color-color diagram for the stellar objects in the survey area. For clarity, we have included in Figure 1 only objects with $B < 21.0$ and present half the error bars. The great majority of objects lie along the stellar locus, which runs from the upper left at ($U - B \sim -0.3$, $B - R \sim 0.7$) to ($U - B \sim 1.5$, $B - R \sim 2.5$). The outliers blueward of the stellar locus in both $U - B$ and $B - R$ are most likely to be QSOs. We chose the boundaries for our QSO candidates based on both visual inspection of Figure 1, which clearly shows the edge of the bulk of the stellar locus, and color-color regions used by similar surveys in the literature. Following the work of Hall et al. (1996), we adopted a two-stage color selection process as follows: we consider QSO candidates to be (1) all objects bluer than $B - R = 0.8$, and (2) all objects with both $U - B \leq -0.4$ and $B - R \leq 1.1$. The boundary in color space of the candidate selection region is represented in Figure 1 by the bent solid line.

Given our two-tiered color-color selection strategy, it is natural to divide our candidate selection region into three rectangular sub-regions. As shown in Figure 1, the area “Q1” is bounded by $U - B < -0.4$ and $B - R < 0.8$, and contains most of the candidates. Areas “Q2” ($U - B > -0.4$ and $B - R < 0.8$) and “Q3” ($U - B > -0.4$ and $0.8 < B - R < 1.1$) together contain about half the number of candidates in “Q1.”

3. QUASARS IN THE DIRECTION OF THE HDF

3.1. Spectroscopy of QSO Candidates

Slit spectroscopy of the QSO candidates was obtained with the Multiple Mirror Telescope between April 1997 and February 1998. Depending on the observing run, either the Blue Channel Spectrograph (3200-8000 Å coverage, 6 Å resolution) or the Red Channel Spectrograph (3700-7400 Å coverage, 10 Å resolution) was used with a 300 l mm⁻¹ grating. As with the photometry, the data were reduced using the standard methods in the *ccdred* and *longslit* packages in IRAF. Although not all the nights were photometric, relative spectrophotometry was obtained for all spectra using the spectrophotometric standards in Massey & Gronwall (1990).

Since our primary scientific goal was to find QSOs bright enough to serve as background probes, we chose a practical limit of $B \sim 21$, corresponding roughly to the faintest QSO that can be measured at high resolution within a few hours using the largest ground-based telescopes. We thus began by observing all candidates brighter than $B = 21.2$ within a 10' radius of the HDF. Then we observed the brightest candidates in the entire square degree, moving progressively fainter as observing time and conditions allowed. Over the course of some 14 partial nights, with widely varying conditions of transparency and seeing, we observed a total of 61 candidates in the two-color region described above. This number comprises all the stellar objects in that region within the survey area from $16 \leq B \leq 20.5$, several fainter targets, and all such targets with $B \leq 21.1$ within 10' of the HDF.

We chose restrictive boundaries for the two-color selection in order to maximize the efficiency in the QSO selection and to produce a relatively complete spectroscopic sample. But the work of Hall et al. (1996), Kennefick et al. (1997) and others have shown that in a UV-excess color plot such as one we use, the region near the end of the stellar locus, though more strongly contaminated by blue stars, can potentially yield additional high-redshift ($z > 2.5$) QSOs. In the hope of confirming even a few such high-redshift QSOs, we obtained spectra of an additional 29 randomly selected objects that were redward of the outlier boundary we established – that is, in the approximate color ranges $-0.3 \leq (U - B) < -0.4$ and $0.8 \leq (B - R) < 1.0$. Unfortunately, none of these borderline candidates were found to be QSOs.

3.2. Confirmed QSOs

Our search netted a total of 30 QSOs and 1 AGN. We present the QSO positions, magnitudes, colors and redshifts in Table 1, and their flux-calibrated spectra in Figure 2. The closest object is the AGN, a Seyfert galaxy at $z = 0.135$; all the others have redshift $z = 0.44$ or greater. The most distant QSO we identified lies at $z = 2.98$. All of these QSO identifications were based either on two or more emission lines, or at least one strong, broad emission line which we assumed to be MgII at 2800 Å (where any other choice would have implied another strong line in our spectral window). Since the spectra were all flux-calibrated with relative spectrophotometry, we could also confirm through continuum fitting that the spectra were consistent with a power law energy

distribution. Figure 3 shows the approximate positions on the sky of the confirmed QSOs with respect to the HDF and its flanking fields.

In addition, we present in Table 2 the results of the spectroscopy of the objects in the color-color regions Q1, Q2 and Q3 (see Figure 1) that did not yield positive QSO confirmations, along with their classification as stars, compact galaxies, or unidentified sources. Together, the objects in Tables 1 and 2 comprise all the objects to the left of the bent solid line in Figure 1 that we have observed. For reference, we include the spectra of the four unidentified sources at the end of Figure 2.

Finally, in Table 3 we list the fainter QSO candidates which fall into the outlier region for which we did not obtain spectra, down to a magnitude limit of $B = 22$. The yield of QSOs within this faint list could potentially double the QSO sample presented in this paper. These tables will hopefully be useful for any future spectroscopic followup efforts within the area covered by this survey.

Looking more closely at the distribution of the QSO candidates in color-color space, we find that region Q1 contains 28 of the 30 confirmed QSOs and a 67% fraction of QSOs to candidates. Region Q2 contains 1 AGN and 1 QSO out of 8 candidates, for a 25% fraction of active nuclei; both are relatively low-redshift objects, at $z = 0.135$ and 0.58 respectively. Region Q3 contains only one QSO and a 9% fraction; but that object has the highest redshift in the sample at $z = 2.98$. We have listed in Table 3 the color-color region of each faint candidate, as a possible indication of how likely the candidate is to be a QSO.

3.3. Completeness and QSO Surface Density

As discussed in Section 3 above, every candidate from $16.0 \leq B \leq 20.5$ in the regions Q1, Q2 and Q3 was observed spectroscopically. This totaled 53 objects, 26 of which are confirmed as QSOs. Among the 8 fainter candidates observed, 4 are confirmed as QSOs. So in both subsamples and as a whole, the selection efficiency is about 50%. This fraction matches the 46% efficiency achieved by Kennefick et al. (1997) in the magnitude range $16.5 < B < 21.0$, using very similar color criteria with their UBV data.

There are 21 candidates with $20.6 \leq B \leq 21.0$ fitting our color criteria for which we have no spectra. If we assume that our observational efficiency is well represented by the 4 out of 8 faint candidates that are confirmed as QSOs, the entire square degree of this survey should contain a total of $\sim 41 \pm 6$ QSOs in this magnitude range. This prediction is entirely consistent with the observations of Kennefick et al. (1997), and with predictions from the results of Koo & Kron (1988) and Boyle, Shanks & Peterson (1988). The fractions of $z < 2.3$ and $z > 2.3$ QSOs that we observe are 27/30 and 3/30, respectively, which is also consistent at the 1σ level with the above authors. This work is not intended as a study of the quasar luminosity function, nor is completeness required to use these QSOs as absorption probes. However, the consistency of our

numbers with those in the literature means that this catalog fairly represents the QSO population in the survey area, and that it has not omitted a large fraction of the QSOs in our magnitude range.

4. SUMMARY

We have surveyed the square degree centered on the Hubble Deep Field for QSOs which can be used as absorption probes, using a straightforward optical multi-color selection technique. We present the results of our spectroscopic identifications, which include 30 confirmed QSOs and 1 AGN in the magnitude range $17.6 < B < 21.0$ and the redshift range $0.14 < z < 2.98$. We also include a list of quasar candidates for which spectroscopy has not yet been obtained. It is our hope that this work will serve as a starting point for the establishment of a detailed grid of absorption probes, in order to study the non-luminous matter within Hubble Deep Field volume and its relationship to the galaxy distribution.

This work was supported by a NASA archival grant for the HST (AR-06337) to the University of Arizona. We thank Paul Hewett for insights into the quasar-hunting business. Additionally, CTL gratefully acknowledges support from NSF grant AST96-17177 to Columbia University.

Table 1. Spectroscopic Results – QSOs

Number	Object ID	R.A. (1950)	Dec. (1950)	B	U-B	B-R	z	Notes
1	Q1230+6226	12 30 12.9	62 26 23	19.4	-0.95	0.41	2.07	$\text{Ly}\alpha, \text{C IV}, \text{C III}$
2	Q1230+6215	12 30 43.6	62 15 34	19.4	-0.84	0.71	1.47	$\text{C IV}, \text{C III}$
3	Q1230+6225	12 30 47.6	62 25 49	18.9	-0.59	0.62	1.83	$\text{Si IV}/\text{O VI}, \text{C IV}, \text{C III}$
4	Q1230+6249	12 30 59.7	62 49 44	20.5	-0.53	0.70	0.80	$\text{C III}, \text{Mg II}$
5	Q1231+6249	12 31 17.5	62 49 26	20.4	-0.87	0.70	1.32	$\text{C IV}, \text{C III}$
6	Q1231+6227	12 31 23.8	62 27 39	20.3	-0.68	0.71	0.50	Mg II
7	Q1231+6249	12 31 45.9	62 49 47	19.9	-0.82	0.59	1.12	$\text{C III}, \text{Mg II}$
8	Q1231+6244	12 31 47.3	62 44 24	19.5	-0.79	0.78	1.31	$\text{C III}, \text{Mg II}$
9	Q1231+6215	12 31 56.3	62 15 05	19.1	-0.68	0.77	1.95	$\text{Ly}\alpha, \text{C IV}, \text{C III}$
10	Q1231+6243	12 31 59.7	62 43 12	17.6	-0.88	0.70	1.33	$\text{C III}, \text{Mg II}$
11	Q1232+6207	12 32 57.9	62 07 28	20.6	-0.66	0.57	0.98	$\text{C III}, \text{Mg II}$
12	Q1233+6221	12 33 55.9	62 21 06	20.5	-0.79	0.68	1.74	$\text{Ly}\alpha, \text{C IV}$
13	Q1234+6231	12 34 08.8	62 31 58	21.0	-0.43	0.66	2.58	$\text{Ly}\alpha, \text{C IV}, \text{C III}$
14	Q1234+6214	12 34 23.3	62 14 45	19.4	-0.43	0.73	2.52	$\text{Ly}\alpha, \text{C IV}, \text{C III}$
15	Q1235+6219	12 35 02.3	62 19 54	20.3	-0.92	0.67	2.05	$\text{Ly}\alpha, \text{C IV}, \text{C III}$
16	Q1235+6205	12 35 33.7	62 05 48	19.1	-0.61	0.64	2.28	$\text{Ly}\alpha, \text{C IV}$
17	Q1235+6230	12 35 47.6	62 30 06	19.2	-0.80	0.74	0.44	$\text{Mg II}, \text{H}\beta$
18	Q1235+6243	12 35 59.2	62 43 56	20.8	-0.49	0.63	0.77	$\text{C III}, \text{Mg II}$
19	Q1236+6241	12 36 02.7	62 41 08	20.9	-0.66	0.69	1.75	$\text{Ly}\alpha, \text{C IV}$
20	Q1236+6218	12 36 02.9	62 18 38	19.3	-0.64	0.58	1.00	$\text{C III}, \text{Mg II}$
21	Q1236+6203	12 36 10.6	62 03 42	20.0	-0.28	0.79	2.98	$\text{Ly}\alpha, \text{C IV}$
22	Q12364+6200	12 36 21.5	62 00 38	20.1	-0.61	0.57	2.27	$\text{Ly}\alpha, \text{C IV}, \text{C III}$
23	Q12366+6200	12 36 35.4	62 00 23	18.2	-0.60	0.61	0.83	$\text{C III}, \text{Mg II}$
24	Q1236+6158	12 36 49.2	61 58 39	20.3	-0.47	0.70	0.91	Mg II
25	Q1237+6222	12 37 19.0	62 22 47	19.6	-0.65	0.68	1.19	$\text{C IV}, \text{C III}$
26	Q1237+6249	12 37 22.2	62 49 47	20.1	-0.56	0.72	1.66	$\text{Ly}\alpha, \text{C IV}, \text{C III}$
27	Q1238+6239	12 38 21.5	62 39 56	20.5	-0.58	0.70	1.09	$\text{C III}, \text{Mg II}$
28	Q1238+6232	12 38 22.3	62 32 33	20.4	-0.59	0.98	0.58	$\text{Mg II}, \text{O II}, \text{H}\delta$
29	Q1238+6252	12 38 36.8	62 52 21	19.3	-0.66	0.55	1.78	$\text{Ly}\alpha, \text{C IV}$
30	Q1238+6205	12 38 45.9	62 05 03	20.1	-0.71	0.58	1.08	$\text{C III}, \text{Mg II}$

Table 2. Spectroscopic Results – non-QSOs

R.A. (1950)	Dec. (1950)	B	U-B	B-R	ID
12 32 14.8	62 34 38	17.8	-0.41	0.84	AGN, z=0.135
12 36 36.1	62 08 45	19.6	-0.32	0.79	?
12 32 13.2	62 23 03	20.5	-0.48	0.81	?
12 33 14.2	62 49 00	20.8	-0.68	0.68	?
12 38 39.4	62 53 01	20.9	-0.57	0.76	?
12 35 59.0	62 39 08	20.4	-0.41	0.80	galaxy, z=0.232
12 36 58.1	62 18 46	16.8	-1.13	0.09	star
12 33 47.9	62 05 06	17.1	-0.35	0.58	star
12 37 41.3	62 24 23	18.2	-0.37	0.77	star
12 38 38.9	62 52 15	18.4	-0.65	0.31	star
12 31 26.6	62 24 30	18.9	-0.27	0.78	star
12 35 35.5	62 00 13	19.1	-0.48	0.91	star
12 37 39.6	62 07 24	19.4	-0.89	0.34	star
12 34 27.8	62 52 48	19.5	-0.31	0.79	star
12 37 41.9	62 16 24	19.6	-0.32	0.75	star
12 33 30.1	62 50 45	19.7	-1.04	0.22	star
12 34 11.5	62 50 53	19.8	-0.43	0.58	star
12 36 07.7	62 35 09	20.0	-0.09	0.65	star
12 35 39.4	62 32 58	20.0	-0.52	1.03	star
12 32 49.5	62 21 50	20.0	-0.79	0.45	star
12 30 44.8	62 19 40	20.0	-0.41	0.61	star
12 32 08.7	62 33 07	20.2	-0.36	0.75	star
12 36 09.4	62 55 57	20.3	-1.06	0.17	star
12 30 04.1	62 38 13	20.4	-0.34	0.75	star
12 33 48.7	62 30 08	20.4	-0.45	0.81	star
12 36 40.5	62 53 13	20.4	-0.42	0.64	star
12 35 51.2	62 26 45	20.5	-0.38	0.68	star
12 33 09.7	62 06 28	20.5	-0.67	0.52	star
12 32 55.1	62 49 25	20.5	-0.48	0.83	star
12 38 22.3	62 51 24	20.9	-0.48	0.73	star
12 34 31.5	62 28 44	21.0	-0.92	0.34	star

Table 3. QSO candidates

R.A. (1950)	Dec. (1950)	B	U-B	B-R	Region
12 31 36.0	63 00 21	20.6	-0.43	0.99	Q3
12 30 53.4	62 04 30	20.6	-0.77	0.60	Q1
12 30 53.5	62 17 35	20.7	-0.85	0.54	Q1
12 30 45.1	62 48 51	20.7	-0.57	0.73	Q1
12 38 19.8	62 18 34	20.8	-0.06	0.76	Q2
12 37 17.7	62 11 02	20.8	-0.51	0.94	Q3
12 37 56.6	62 18 48	20.8	-0.40	0.77	Q2
12 38 53.6	62 23 15	20.9	-0.44	1.06	Q3
12 33 17.7	62 30 01	20.9	-0.34	0.67	Q2
12 35 48.4	62 36 50	20.9	-0.47	0.74	Q1
12 37 14.4	62 50 32	20.9	-0.88	0.73	Q1
12 34 53.2	62 42 20	20.9	-0.58	1.01	Q3
12 38 56.9	61 58 32	20.9	-0.58	0.76	Q1
12 37 49.7	62 25 07	21.0	-0.49	0.68	Q1
12 38 58.9	62 21 59	21.0	-0.18	0.67	Q2
12 32 24.4	62 24 00	21.0	-0.64	0.66	Q1
12 35 18.1	62 39 36	21.0	-0.46	0.83	Q3
12 30 33.7	62 14 17	21.0	-0.52	0.61	Q1
12 31 18.7	62 25 36	21.0	-0.30	0.75	Q2
12 35 17.2	62 18 51	21.0	-0.63	0.74	Q1
12 36 35.1	62 30 55	21.0	-0.68	0.48	Q1
12 32 26.6	62 43 09	21.1	-0.42	0.75	Q1
12 34 27.6	62 21 12	21.1	-0.44	0.80	Q3
12 31 41.0	62 29 58	21.1	-0.31	0.66	Q2
12 33 48.2	62 50 05	21.1	-0.53	0.88	Q3
12 31 22.8	62 10 19	21.1	-1.06	0.57	Q1
12 37 24.3	62 22 01	21.1	-0.47	0.89	Q3
12 30 41.4	62 32 18	21.1	-0.61	0.66	Q1
12 37 07.5	62 00 35	21.1	-0.45	0.77	Q1
12 35 51.8	62 45 59	21.1	-0.88	0.55	Q1
12 33 56.1	62 33 01	21.2	-0.62	0.80	Q3
12 32 18.1	62 31 46	21.2	-0.65	0.62	Q1
12 31 21.9	62 52 44	21.2	-0.70	1.03	Q3
12 36 40.0	62 19 07	21.2	-0.34	0.76	Q2
12 34 35.9	62 46 04	21.2	-0.37	0.62	Q2
12 31 40.1	62 44 34	21.2	-0.44	0.82	Q3
12 31 42.7	62 56 23	21.2	-0.10	0.73	Q2
12 30 23.0	62 27 23	21.2	-0.96	0.64	Q1
12 32 50.8	62 09 15	21.2	-1.16	0.26	Q1
12 31 21.6	62 26 59	21.2	-0.47	0.77	Q1
12 36 55.7	62 33 39	21.2	-0.56	0.86	Q3
12 31 42.1	62 16 04	21.3	-0.82	1.01	Q3
12 35 10.0	62 58 34	21.3	-0.53	1.08	Q3
12 38 58.9	62 51 39	21.3	-0.90	0.90	Q3
12 33 58.0	62 36 13	21.3	-0.99	0.44	Q1
12 35 54.2	62 48 21	21.3	-0.43	0.97	Q3
12 36 26.6	62 17 13	21.3	-0.28	0.74	Q2
12 36 45.1	62 23 46	21.3	-0.36	0.68	Q2
12 31 54.5	62 06 43	21.3	-0.49	0.75	Q1
12 38 17.3	62 50 23	21.3	-0.48	0.94	Q3
12 34 05.9	62 47 34	21.4	-0.72	0.77	Q1
12 38 07.2	62 05 09	21.4	-0.24	0.62	Q2

Table 3—Continued

R.A. (1950)	Dec. (1950)	B	U-B	B-R	Region
12 31 25.0	62 22 03	21.4	-0.49	0.82	Q3
12 33 28.5	62 25 06	21.4	-0.61	0.97	Q3
12 35 31.5	62 13 42	21.4	-0.43	1.07	Q3
12 32 13.0	62 24 55	21.4	-1.15	0.59	Q1
12 32 51.3	61 59 33	21.4	-0.41	1.05	Q3
12 35 07.4	62 08 03	21.4	-2.11	-.16	Q1
12 32 22.5	62 48 54	21.4	-0.53	0.91	Q3
12 34 23.8	62 01 14	21.4	-0.56	0.65	Q1
12 31 54.7	62 23 08	21.4	-0.12	0.78	Q2
12 38 56.4	62 05 04	21.4	-0.45	1.03	Q3
12 31 17.9	62 52 46	21.4	-0.64	0.94	Q3
12 31 15.7	62 41 09	21.4	-0.76	0.58	Q1
12 35 40.1	62 10 15	21.5	-0.28	0.76	Q2
12 37 19.3	62 34 16	21.5	-0.51	0.83	Q3
12 30 57.6	62 09 18	21.5	-0.73	0.42	Q1
12 30 57.0	62 14 06	21.5	-0.33	0.76	Q2
12 36 11.7	62 09 06	21.5	-0.55	0.57	Q1
12 31 59.8	62 11 33	21.5	-0.50	0.63	Q1
12 33 16.9	62 09 06	21.5	-0.68	0.90	Q3
12 36 03.2	62 38 20	21.5	-0.42	0.93	Q3
12 35 53.1	62 29 53	21.5	-0.50	0.86	Q3
12 36 23.9	62 20 26	21.5	-0.63	1.01	Q3
12 30 34.0	62 40 42	21.5	-0.15	0.62	Q2
12 35 51.9	62 04 45	21.6	-0.43	0.96	Q3
12 30 19.9	62 28 37	21.6	-1.00	0.10	Q1
12 34 51.1	62 31 25	21.6	-0.39	0.73	Q2
12 39 00.9	62 29 44	21.6	-0.50	0.98	Q3
12 37 01.8	62 26 25	21.6	-0.56	0.86	Q3
12 30 56.6	62 20 14	21.6	-0.70	0.90	Q3
12 36 03.2	62 46 44	21.6	-0.86	0.60	Q1
12 34 51.5	62 20 33	21.6	-0.47	0.79	Q1
12 34 53.0	62 47 50	21.6	-0.75	0.68	Q1
12 30 47.9	62 11 39	21.6	-0.88	0.78	Q1
12 34 16.7	62 42 44	21.6	-0.33	0.73	Q2
12 31 29.4	62 34 20	21.6	-0.37	0.79	Q2
12 30 31.7	62 28 59	21.6	-0.50	0.91	Q3
12 30 13.2	62 23 02	21.6	-0.42	1.08	Q3
12 35 02.6	62 56 35	21.6	-0.45	0.73	Q1
12 31 54.6	62 40 11	21.6	-0.50	0.88	Q3
12 31 03.9	62 34 42	21.6	-0.53	0.89	Q3
12 32 52.4	62 38 11	21.6	-0.75	0.93	Q3
12 32 18.4	62 09 43	21.6	-0.76	0.97	Q3
12 35 46.7	62 56 26	21.6	-0.72	0.89	Q3
12 37 07.6	62 15 08	21.6	-0.74	0.80	Q3
12 31 05.3	62 03 44	21.6	-1.45	0.89	Q3
12 34 32.5	62 44 24	21.7	-0.44	0.87	Q3
12 32 55.5	62 41 20	21.7	-0.50	0.77	Q1
12 30 39.4	62 47 53	21.7	-0.96	0.84	Q3
12 35 33.6	62 45 25	21.7	-0.44	1.09	Q3
12 36 25.7	62 21 13	21.7	-0.41	0.91	Q3
12 33 34.4	62 39 02	21.7	-0.52	0.92	Q3
12 30 23.8	62 55 47	21.7	-0.48	1.01	Q3

Table 3—Continued

R.A. (1950)	Dec. (1950)	B	U-B	B-R	Region
12 32 27.2	62 24 47	21.7	-0.42	0.81	Q3
12 32 19.7	62 33 36	21.7	-0.47	0.93	Q3
12 35 44.0	62 14 05	21.7	-0.59	0.71	Q1
12 35 53.5	61 59 10	21.7	-0.78	0.69	Q1
12 31 08.0	62 45 25	21.7	-0.81	0.94	Q3
12 36 20.5	62 20 21	21.7	-1.05	0.46	Q1
12 35 47.9	62 58 37	21.7	-0.55	0.75	Q1
12 31 55.4	62 31 01	21.7	-0.72	0.62	Q1
12 35 35.6	62 26 41	21.8	-0.54	1.04	Q3
12 30 24.8	62 26 29	21.8	-0.69	0.55	Q1
12 34 13.3	62 26 50	21.8	-0.36	0.78	Q2
12 34 37.9	62 34 06	21.8	-0.46	0.81	Q3
12 38 08.9	62 35 25	21.8	-0.54	0.65	Q1
12 34 29.6	62 38 33	21.8	-0.60	0.82	Q3
12 31 19.6	62 07 59	21.8	-0.93	0.45	Q1
12 35 54.7	62 37 14	21.8	-0.19	0.72	Q2
12 34 05.1	62 07 32	21.8	-0.44	0.58	Q1
12 30 18.2	62 22 10	21.8	-0.44	0.95	Q3
12 33 40.9	62 21 06	21.8	-0.73	0.87	Q3
12 34 44.5	62 52 02	21.8	-0.41	0.87	Q3
12 36 09.8	62 40 31	21.8	-0.41	0.91	Q3
12 33 44.1	62 34 29	21.8	-0.51	0.66	Q1
12 34 18.5	62 41 21	21.8	-0.66	1.02	Q3
12 37 35.1	62 04 30	21.8	-1.64	0.35	Q1
12 31 01.6	62 19 36	21.8	-0.51	0.78	Q1
12 34 43.8	62 45 53	21.8	-1.11	0.90	Q3
12 34 04.4	62 27 46	21.8	-0.92	0.72	Q1
12 31 58.3	62 35 08	21.9	-0.33	0.68	Q2
12 36 51.1	62 21 33	21.9	-0.79	0.72	Q1
12 35 48.2	62 54 22	21.9	-0.89	0.51	Q1
12 34 34.5	62 24 24	21.9	-0.31	0.74	Q2
12 34 50.5	62 02 18	21.9	-0.62	0.53	Q1
12 31 18.1	62 43 23	21.9	-0.54	0.80	Q3
12 31 55.0	62 19 32	21.9	-0.45	0.89	Q3
12 35 03.2	62 22 24	21.9	-0.77	0.67	Q1
12 36 12.0	62 46 07	21.9	-0.61	0.98	Q3
12 36 06.6	62 49 14	21.9	-0.95	0.79	Q1
12 31 59.5	62 23 23	21.9	-0.35	0.72	Q2
12 31 12.7	62 29 48	22.0	-1.01	0.80	Q3
12 32 57.4	62 52 10	22.0	-1.05	0.20	Q1
12 37 00.7	62 09 14	22.0	-1.09	0.50	Q1
12 36 02.9	62 23 00	22.0	-0.48	0.98	Q3
12 35 23.3	62 42 54	22.0	-0.70	0.54	Q1
12 32 27.9	62 48 29	22.0	-0.93	1.00	Q3
12 32 58.6	62 19 31	22.0	-0.48	0.98	Q3
12 32 07.5	62 40 56	22.0	-0.71	1.01	Q3
12 30 53.6	62 30 26	22.0	-0.81	0.99	Q3

REFERENCES

Boyle, B.J., Shanks, T., & Peterson, B.A. 1988, MNRAS, 235, 935

Cen, R., Phelps, S., Miralda-Escudé, J., & Ostriker, J.P. 1998, ApJ, 496, 577

Cohen, J.G., Cowie, L.L., Hogg, D.W., Songaila, A., Blandford, R.D., Hu, E.M., & Shopbell, P. 1996, ApJ, 471, L5

Cohen, J.G., Blandford, R.D., Hogg, D.W., Pahre, M.A., & Shopbell, P.L. 1999, ApJ, 512, 30

Dinshaw, N., & Impey, C.D. 1996, ApJ, 458, 73

Hall, P.B., Osmer, P.S., Green, R.F., Porter, A.C., & Warren, S.J. 1996, ApJ, 462, 614

Hernquist, L., Katz, N., Weinberg, D., and Miralda-Escudé, J. 1996, ApJ, 457, 57

Kennefick, J.D., Osmer, P.S., Hall, P.B., & Green, R.F. 1997, AJ, 114, 2269

Koo, D.C., & Kron, R.G. 1988, ApJ, 325, 92

Koo, D.C., Kron, R.G., & Cudworth, K.M. 1986, PASP, 98, 285

Livio, M., Fall, S.M., & Madau, P. 1998, editors, The Hubble Deep Field: Proceedings of the Space Telescope Science Institute Symposium (Cambridge: Cambridge University Press)

Massey, P., & Gronwall, C. 1990, ApJ, 358, 344

Meylan, G. 1995, editor, QSO Absorption Lines: Proceedings of the ESO Workshop (Berlin: Springer-Verlag)

Miralda-Escudé, J., Cen, R., Ostriker, J.P., and Rauch, M. 1996, ApJ, 471, 582

Quashnock, J.M., & Vanden Berk, D.E. 1998, ApJ, 500, 28

Rauch, M. 1998, ARA&A, 38, 267

Sargent, W.L.W., & Steidel, C.C. 1987, ApJ, 322, 142

Valdes, F. 1982, FOCAS User's Manual (Tucson: Kitt Peak National Observatory)

Warren, S.J., Hewett, P.C., Irwin, M.J., & Osmer, P.S. 1991, ApJS, 76, 1

Williams, R.E. et al. 1996, AJ, 112, 1335.

Williams, R.E. et al. 1998, Bulletin of the AAS, 193, 7501

Williger, G.M., Hazard, C., Baldwin, J.A., & McMahon, R.G. 1996, ApJS, 104, 145

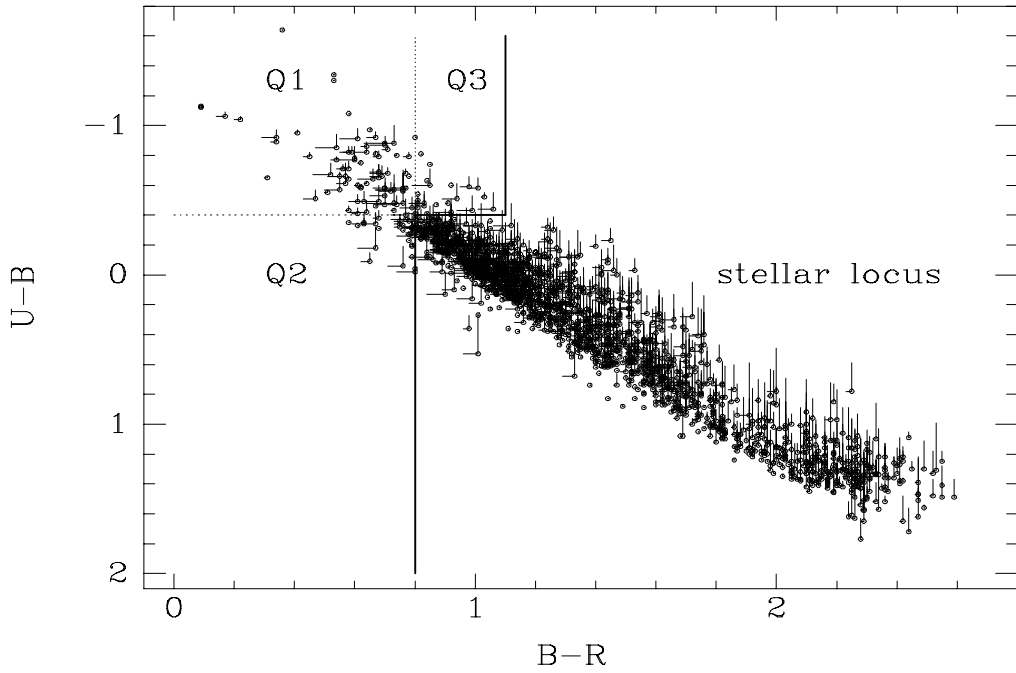


Fig. 1.— $U - B$ vs. $B - R$ diagram for all stellar objects in the survey area with $B < 21.0$. For clarity, only half the error bars are plotted for each data point. The bent solid line denotes the boundary that marks the approximate end of the stellar locus; objects bluer than this have a high probability of being QSOs. The dotted lines mark the boundaries of the color-color regions Q1, Q2 and Q3 (see text).

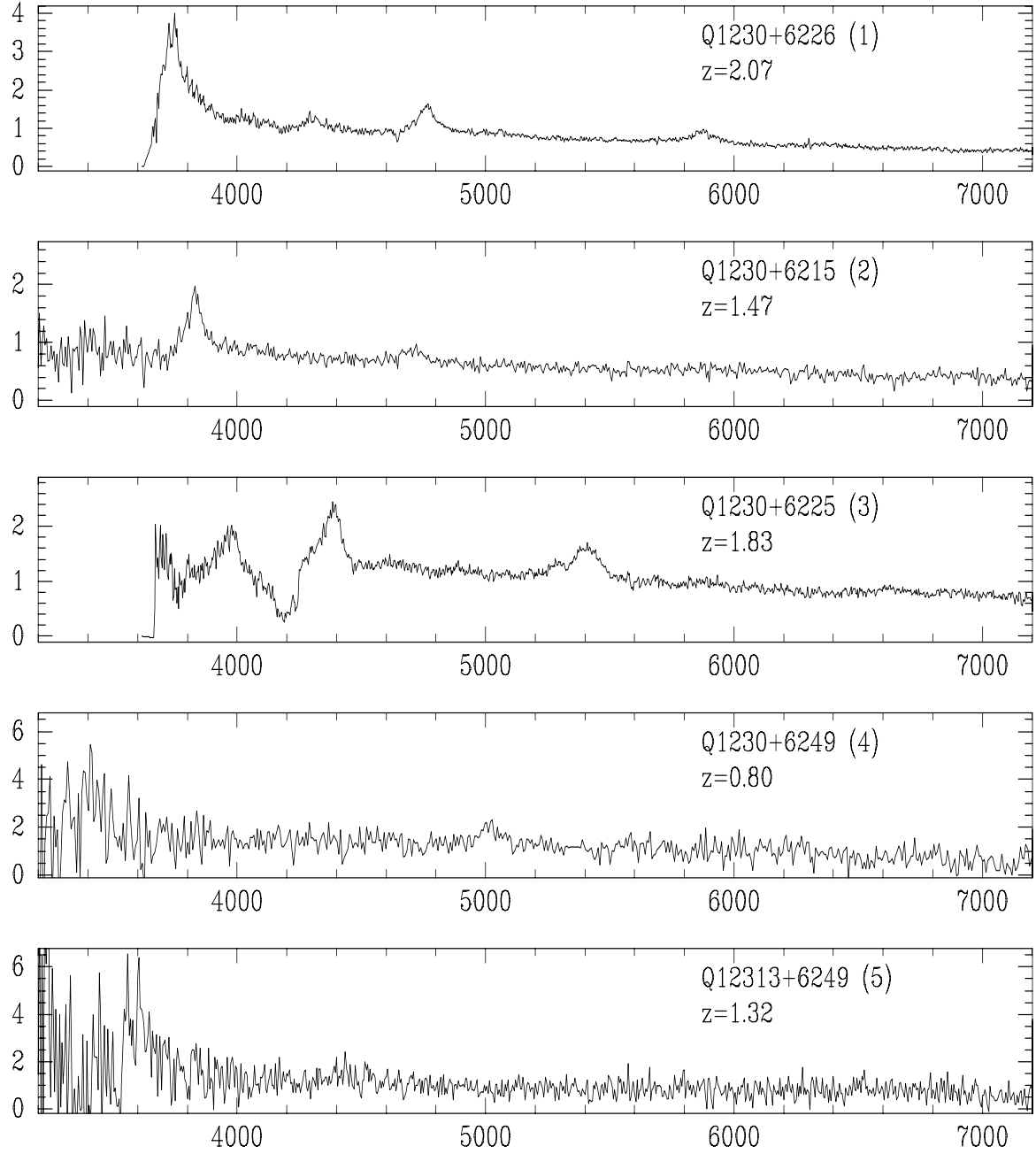
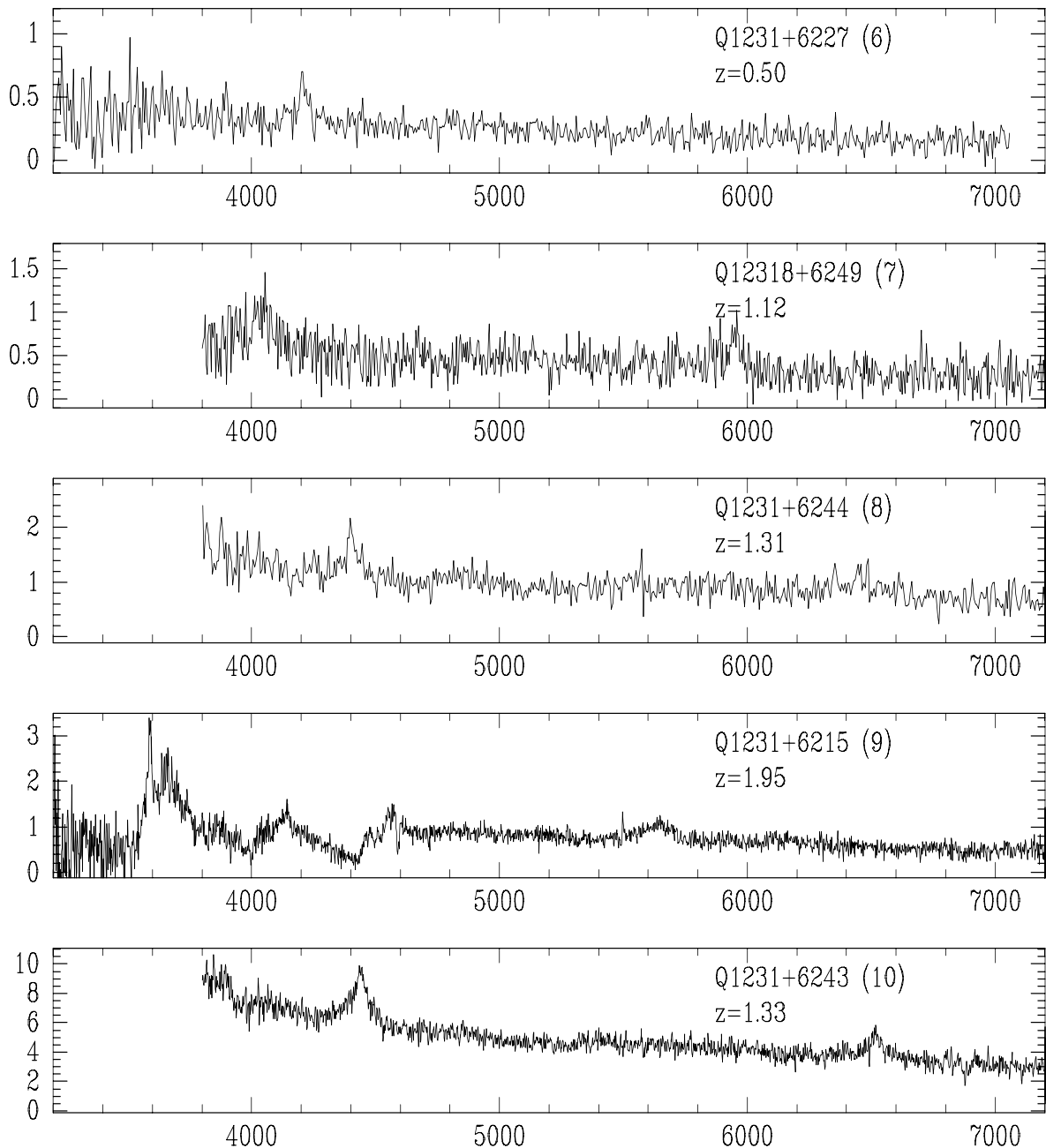
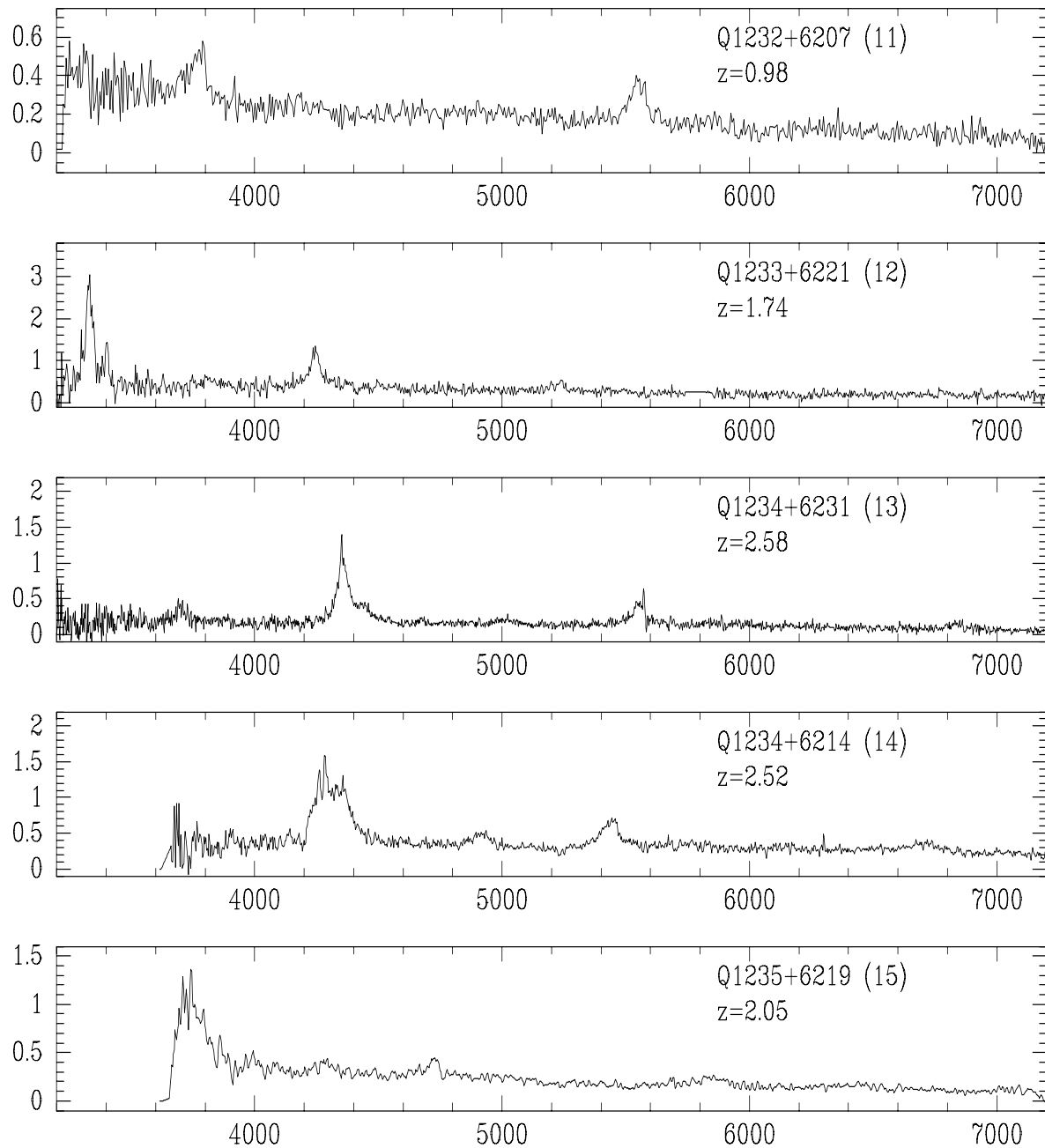
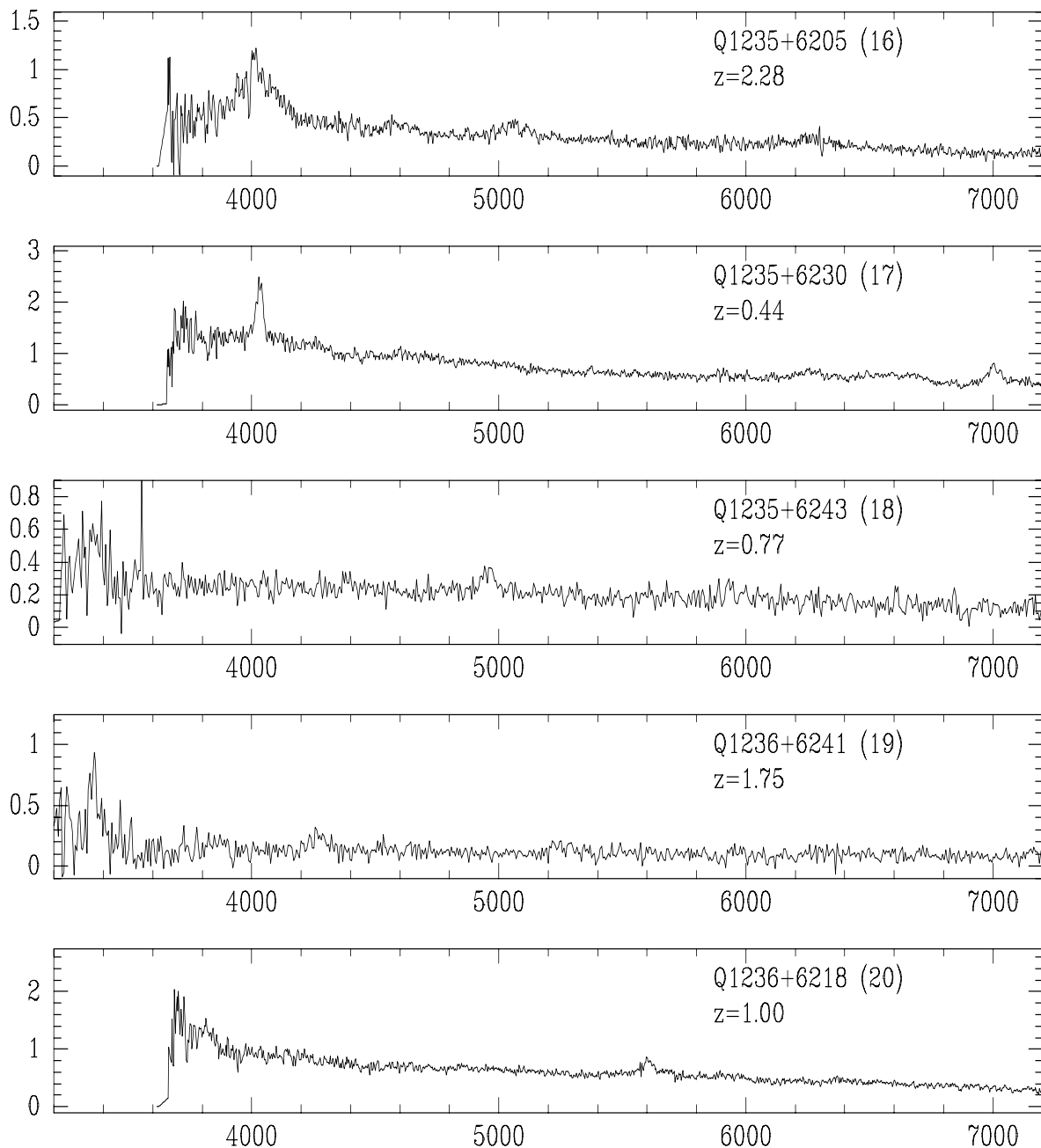
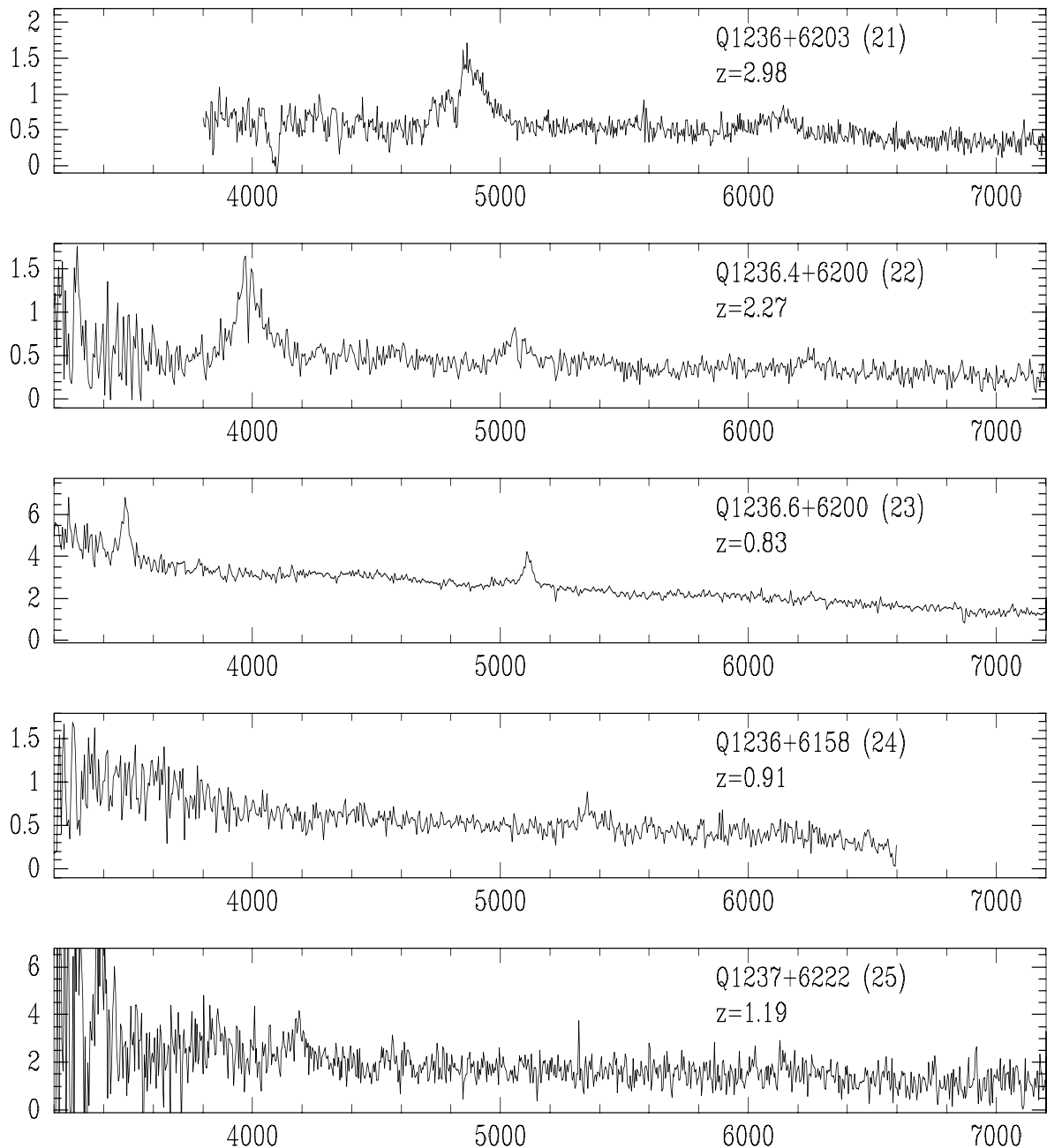


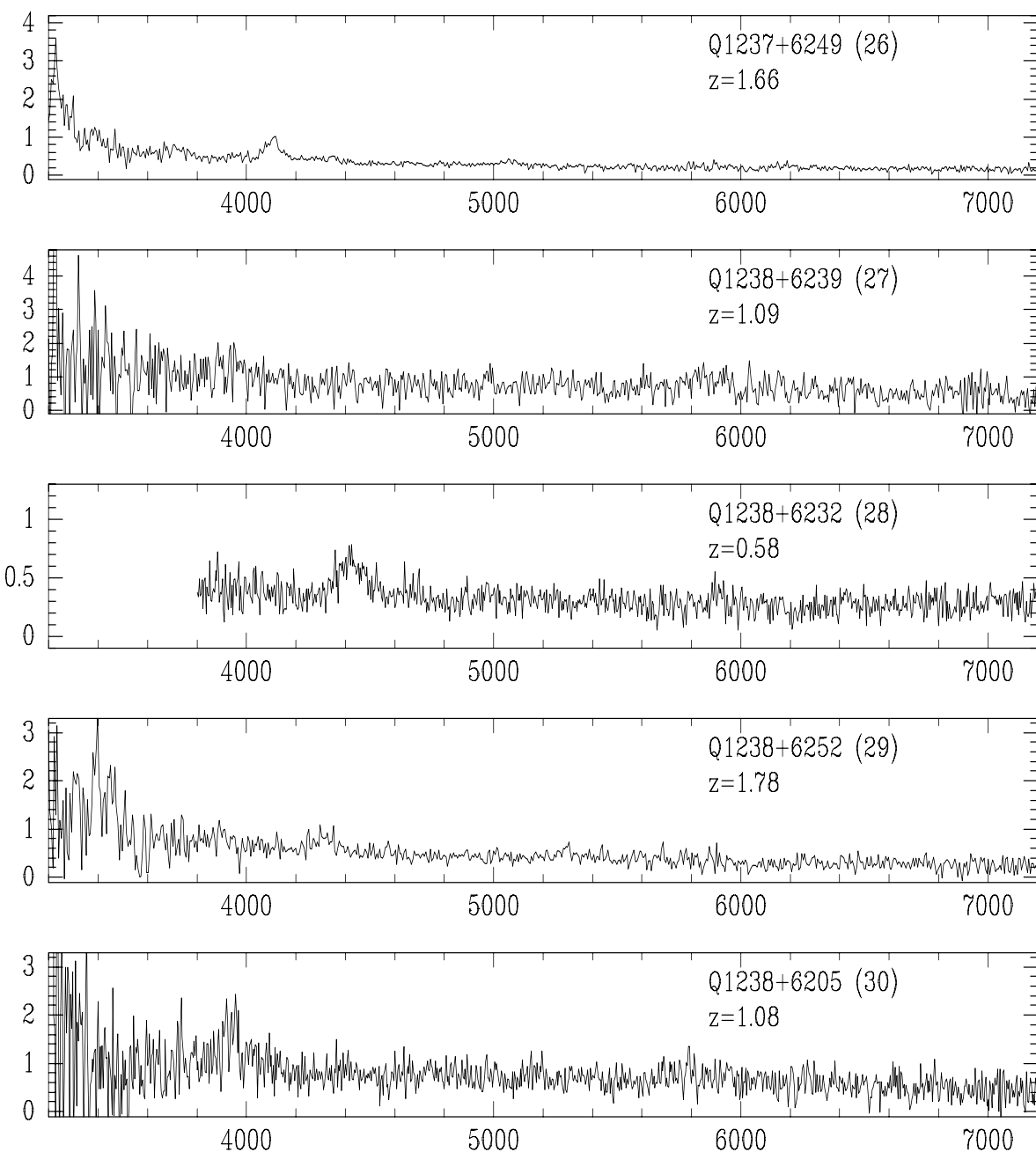
Fig. 2.— Spectra of the QSOs identified from the spectroscopy. Wavelength is in \AA . Flux is presented in units of $10^{-16} \text{ ergs cm}^{-2} \text{ sec}^{-1} \text{ \AA}^{-1}$. Redshifts are based on the detection of two or more broad emission features. The last four spectra have an uncertain classification.

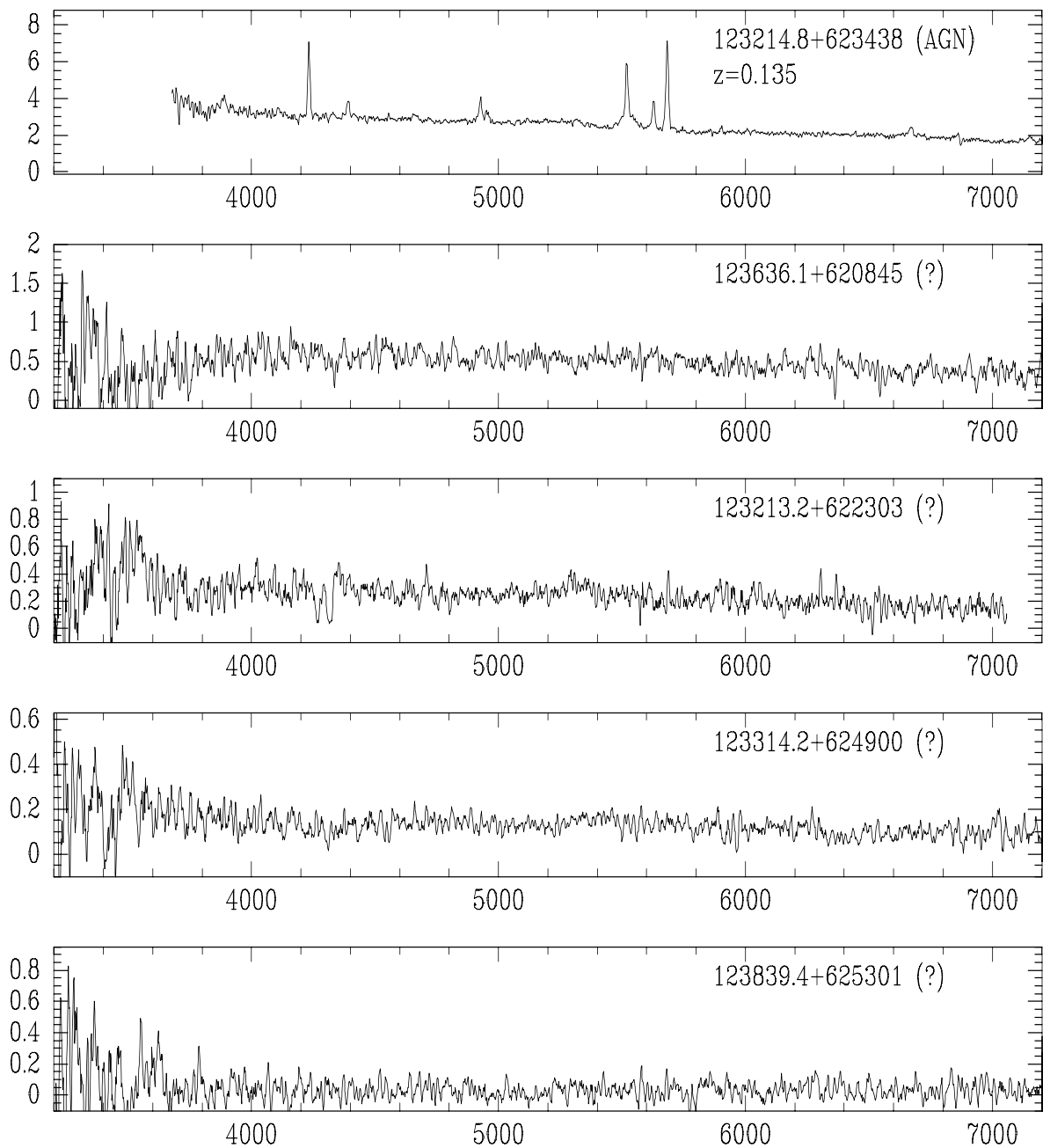












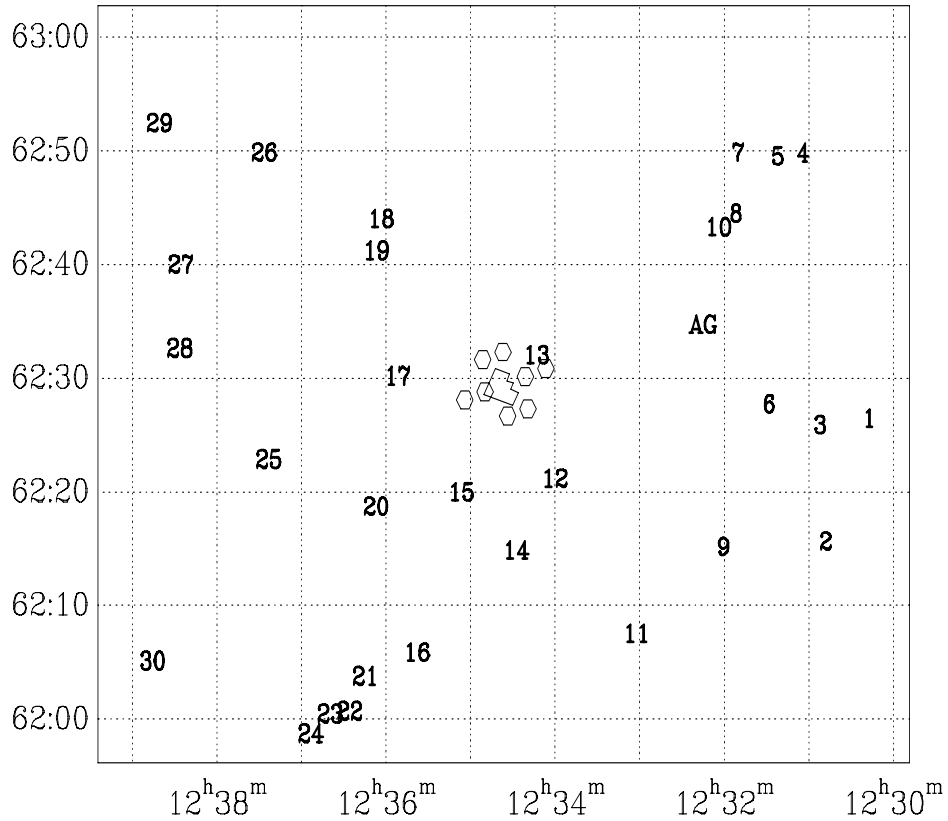


Fig. 3.— Schematic map of the QSOs identified in Table 1, relating their approximate positions with the Hubble Deep Field at the center. The hexagons mark the centers of the HDF flanking fields. The active galaxy at $z=0.135$ is marked as “AG.” R.A. and Dec. are B1950.0.